Atmospheric
Chemistry
and Physics

Open Access

EGU

Supplement of

Ice-nucleating ability of aerosol particles and possible sources at three coastal marine sites

Meng Si et al.

Correspondence to: Allan K. Bertram (bertram@chem.ubc.ca)

Supplemental material

S1 Conversion of mobility diameter measured at Labrador Sea and Lancaster Sound to aerodynamic diameter

The SMPS measured mobility diameter rather than aerodynamic diameter, while both the APS and the MOUDI measured aerodynamic diameter. To allow comparison between the SMPS data, the APS data and the INP data, the mobility diameter, D_m, measured by the SMPS was converted to aerodynamic diameter, D_{ae}, using the following equation (Khlystov et al., 2004):

$$D_{ae} = \sqrt{\frac{\rho_{p,RH}}{\chi \rho_o}} D_m, \tag{S1}$$

where χ is the dynamic shape factor that accounts for the non-spherical particle shape; ρ_o is the unit density of 1 g cm^{-3}; and $\rho_{p,RH}$ is the particle density at the sampling RH. In all cases, we assumed a dynamic shape factor of 1. The particle density at the sampling RH, $\rho_{p,RH}$, was calculated using the following equation:

$$\rho_{p,RH} = \rho_w + (\rho_{p,dry} - \rho_w)\frac{1}{gf^3}, \tag{S2}$$

where ρ_w is the density of water; $\rho_{p,dry}$ is the density of the dry particles; gf is the hygroscopic growth factor. The hygroscopic growth factor was based on the numerical model developed by Ming and Russell (2001) assuming the sampled aerosol consisted of sea spray aerosol with a 30 % organic mass content, following the assumption made in DeMott et al. (2016). This assumption results in growth factors of 1.2 at 70 % RH, and 2.4 at 95 % RH, which are consistent with measurements made in the Arctic summer marine boundary layer by Zhou et al. (2001) (1.23 ± 0.09 at 70 % RH, 2.05 ± 0.11 at 90 % RH). For the density of the dry particles, we also assumed a sea spray aerosol with a 30 % organic mass content, resulting in a dry density of 1.87 g cm^{-3}. To determine the sensitivity of the size distribution to the assumed composition of the aerosol, calculations were also carried out assuming a sea spray aerosol with a 10 % organic mass content and a 50 % organic mass content. The difference in the resulted size distributions assuming 10 %, 30 %, and 50 % organic mass content is small (see Fig. S7); hence, data shown in the main text only correspond to an assumed composition of a sea spray aerosol with a 30 % organic mass content.

S2 Conversion of mobility diameter to aerodynamic diameter and correction for hygroscopic growth at Amphitrite Point

At Amphitrite Point, dryers were used prior to sampling with the SMPS. As a result, SMPS data needs to be corrected for hygroscopic growth, and the mobility diameter needs to be converted to aerodynamic diameter. The equation to correct for hygroscopic growth is the following:

$$D_{m,RH} = gf \times D_{m,dry}, \tag{S3}$$

where, $D_{m,RH}$ is the mobility diameter at the sampling RH; $D_{m,dry}$ is the mobility diameter under dry condition. The relationship between mobility diameter and aerodynamic diameter is given in Eq. (S1). Combining Eq. (S1) and Eq. (S3) results in the following:

$$D_{ae,RH} = gf \sqrt{\frac{\rho_{p,RH}}{\chi \rho_o}} D_{m,dry} = x D_{m,dry}, \tag{S4}$$

where $D_{ae,RH}$ is the aerodynamic diameter at the sampling RH, and $x = gf \sqrt{\frac{\rho_{p,RH}}{\chi \rho_o}}$.

Equation (S4) illustrates that the relationship between the dry mobility diameter and the wet aerodynamic diameter is a simple factor x. To determine x, we varied this factor until the optimum fit was obtained between the SMPS and the APS data where overlap occurred (0.7 to 0.93 µm). This type of approach has been used successfully in the past to merge the SMPS and APS data (Beddows et al., 2010; Khlystov et al., 2004). Note, we did not use this approach in Sect. S1 since there was no overlapping size range between the SMPS and APS data measured at Labrador Sea and Lancaster Sound to allow an optimization of the fit.

S3 Conversion of n_s values based on dry, geometric diameters to n_s values based on wet, aerodynamic diameters

The n_s values of sea spray aerosol reported in DeMott et al. (2016) and the n_s values of mineral dust reported in Niemand et al. (2012) are based on dry, geometric diameters. In the following, we investigated how much n_s values based on dry, geometric diameters ($n_{s\_geo,dry}$) overestimate n_s values based on wet, aerodynamic diameters ($n_{s\_ae,RH}$).

Assuming the particles are all spherical, the mobility diameter of a particle is the same as its geometric diameter. Thus, Eq. (S4) can be written as the following:

$$D_{ae,RH} = gf \sqrt{\frac{\rho_{p,RH}}{\chi \rho_o}} D_{geo,dry} = x D_{geo,dry}, \tag{S5}$$

where $D_{geo,dry}$ is the dry, geometric diameter, and $x = gf \sqrt{\frac{\rho_{p,RH}}{\chi \rho_o}}$.

The n_s values based on wet, aerodynamic diameters can be calculated using the following equation:

$$n_{s\_ae,RH} = \frac{[INPs]}{S_{tot,ae,RH}} = \frac{[INPs]}{\pi D_{ae,RH}^2 N_{tot}} = \frac{[INPs]}{\pi x^2 D_{geo,dry}^2 N_{tot}} = \frac{[INPs]}{x^2 S_{tot,geo,dry}} = \frac{n_{s\_geo,dry}}{x^2}, \tag{S6}$$

where $[INPs]$ is the concentration of INPs; $S_{tot,ae,RH}$ is the total surface area based on wet, aerodynamic diameters; N_{tot} is the total number of aerosol particles, $S_{tot,geo,dry}$ is the total surface area based on dry, geometric diameters.

According to Eq. (S6), n_s values based on dry, geometric diameters overestimate n_s values based on wet, aerodynamic by a factor of x^2.

For sea spray aerosol, we assumed a 30 % organic mass content, which resulted in gf of 2.4, and $\rho_{p,RH}$ of 1.1 g cm^{-3} at the highest sampling RH (95 %) in this study. For these conditions, x^2 is approximately 6.

For mineral dust, we assumed mineral dust is non-hygroscopic (therefore gf is 1) with a density of 2 g cm^{-3} (Khlystov et al., 2004). For these conditions, x^2 is 2.

References:

Beddows, D. C. S., Dall'osto, M. and Harrison, R. M.: An Enhanced Procedure for the Merging of Atmospheric Particle Size Distribution Data Measured Using Electrical Mobility and Time-of-Flight Analysers, Aerosol Sci. Technol., 44(11), 930–

5   938, doi:10.1080/02786826.2010.502159, 2010.

DeMott, P. J., Hill, T. C. J., McCluskey, C. S., Prather, K. A., Collins, D. B., Sullivan, R. C., Ruppel, M. J., Mason, R. H., Irish, V. E., Lee, T., Hwang, C. Y., Rhee, T. S., Snider, J. R., McMeeking, G. R., Dhaniyala, S., Lewis, E. R., Wentzell, J. J. B., Abbatt, J., Lee, C., Sultana, C. M., Ault, A. P., Axson, J. L., Diaz Martinez, M., Venero, I., Santos-Figueroa, G., Stokes, M. D., Deane, G. B., Mayol-Bracero, O. L., Grassian, V. H., Bertram, T. H., Bertram, A. K., Moffett, B. F. and Franc, G. D.:

10   Sea spray aerosol as a unique source of ice nucleating particles, Proc. Natl. Acad. Sci., 113(21), 5797–5803, doi:10.1073/pnas.1514034112, 2016.

Khlystov, A., Stanier, C. and Pandis, S. N.: An Algorithm for Combining Electrical Mobility and Aerodynamic Size Distributions Data when Measuring Ambient Aerosol Special Issue of Aerosol Science and Technology on Findings from the Fine Particulate Matter Supersites Program, Aerosol Sci. Technol., 38(sup1), 229–238,

15   doi:10.1080/02786820390229543, 2004.

Ming, Y. and Russell, L. M.: Predicted hygroscopic growth of sea salt aerosol, J. Geophys. Res. Atmos., 106(D22), 28259–28274, doi:10.1029/2001JD000454, 2001.

Niemand, M., Möhler, O., Vogel, B., Vogel, H., Hoose, C., Connolly, P., Klein, H., Bingemer, H., DeMott, P., Skrotzki, J. and Leisner, T.: A Particle-Surface-Area-Based Parameterization of Immersion Freezing on Desert Dust Particles, J. Atmos.

20   Sci., 69(10), 3077–3092, doi:10.1175/JAS-D-11-0249.1, 2012.

O'Dowd, C. D., Becker, E. and Kulmala, M.: Mid-latitude North-Atlantic aerosol characteristics in clean and polluted air, Atmos. Res., 58(3), 167–185, doi:10.1016/S0169-8095(01)00098-9, 2001.

Zhou, J., Swietlicki, E., Berg, O. H., Aalto, P. P., Hämeri, K., Nilsson, E. D. and Leck, C.: Hygroscopic properties of aerosol particles over the central Arctic Ocean during summer, J. Geophys. Res. Atmos., 106(D23), 32111–32123,

25   doi:10.1029/2000JD900426, 2001.

Table S1. The correction factors $f_{nu,1\,mm}$ and $f_{nu,0.25-0.1\,mm}$ for MOUDI stages 2-8 when using substrate holders. For $f_{nu,1\,mm}$, the numbers in the square brackets are the uncertainties, which aas the standard deviations.

MOUDI Stages	$f_{nu,1\,mm}$	$f_{nu,0.25-0.1\,mm}$
2	0.74, [+0.18, −0.12]	$0.1225\exp(-11.29\mu)+1.065\exp(-0.06412\mu)$
3	0.72, [+0.08, −0.08]	$0.04718\exp(-14.15\mu)+1.023\exp(-0.02347\mu)$
4	1.18, [+0.09, −0.14]	$0.04252\exp(-13.06\mu)+1.024\exp(-0.02386\mu)$
5	0.97, [+0.03, −0.10]	$0.03023\exp(-14.97\mu)+1.015\exp(-0.01515\mu)$
6	0.75, [+0.19, −0.02]	$0.5799\exp(-10.57\mu)+1.148\exp(-0.1408\mu)$
7	0.84, [+0.07, −0.11]	$0.1151\exp(-10.66\mu)+1.072\exp(-0.07029\mu)$
8	1.01, [+0.03, −0.12]	$1.03\exp(-12.79\mu)+1.268\exp(-0.2422\mu)$

$\mu = \frac{N_u(T)}{N_0}$, where $N_u(T)$ is the number of unfrozen droplets at temperature T, and N_0 is the total number of droplets in one freezing experiment.
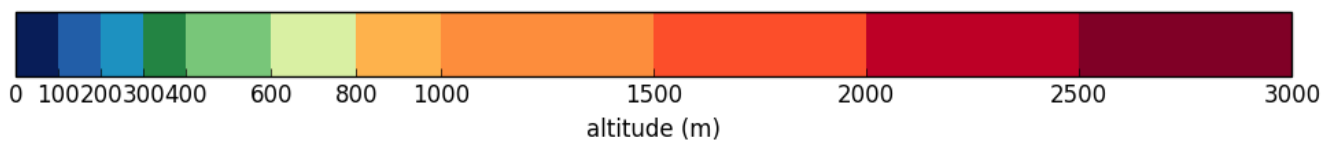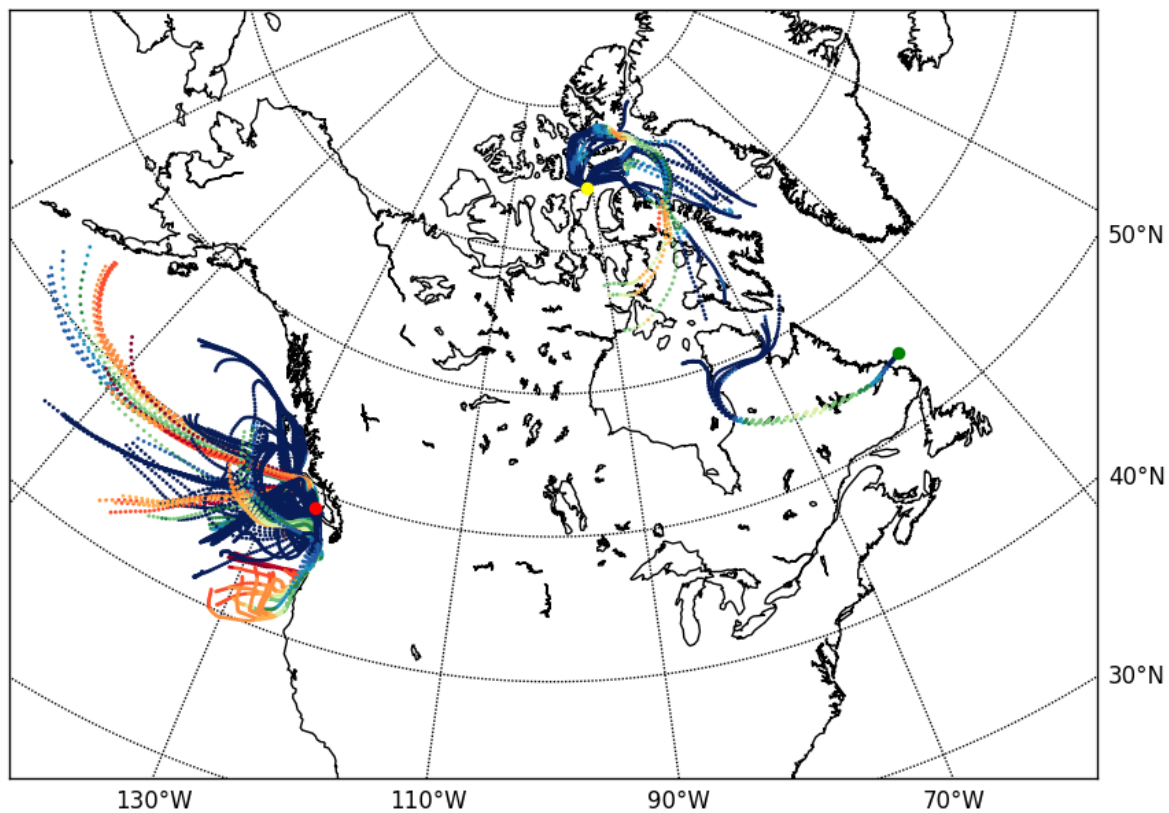
Figure S1. The 3-day HYSPLIT back trajectories initiating at 50 m above ground level for Amphitrite Point (red dot), Labrador Sea (green dot) and Lancaster Sound (yellow dot). The back trajectories were calculated for every hour during the MOUDI sampling period. The starting points are labeled as coloured dots, and the altitude is shown using a colour scale.
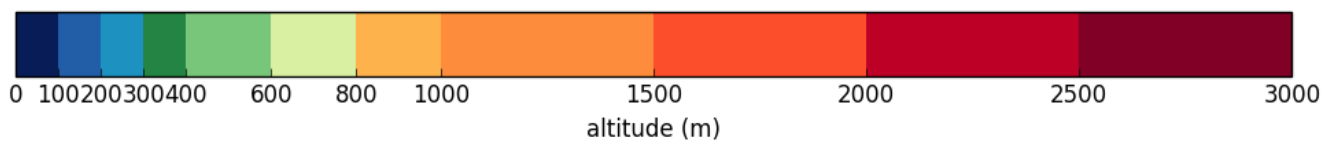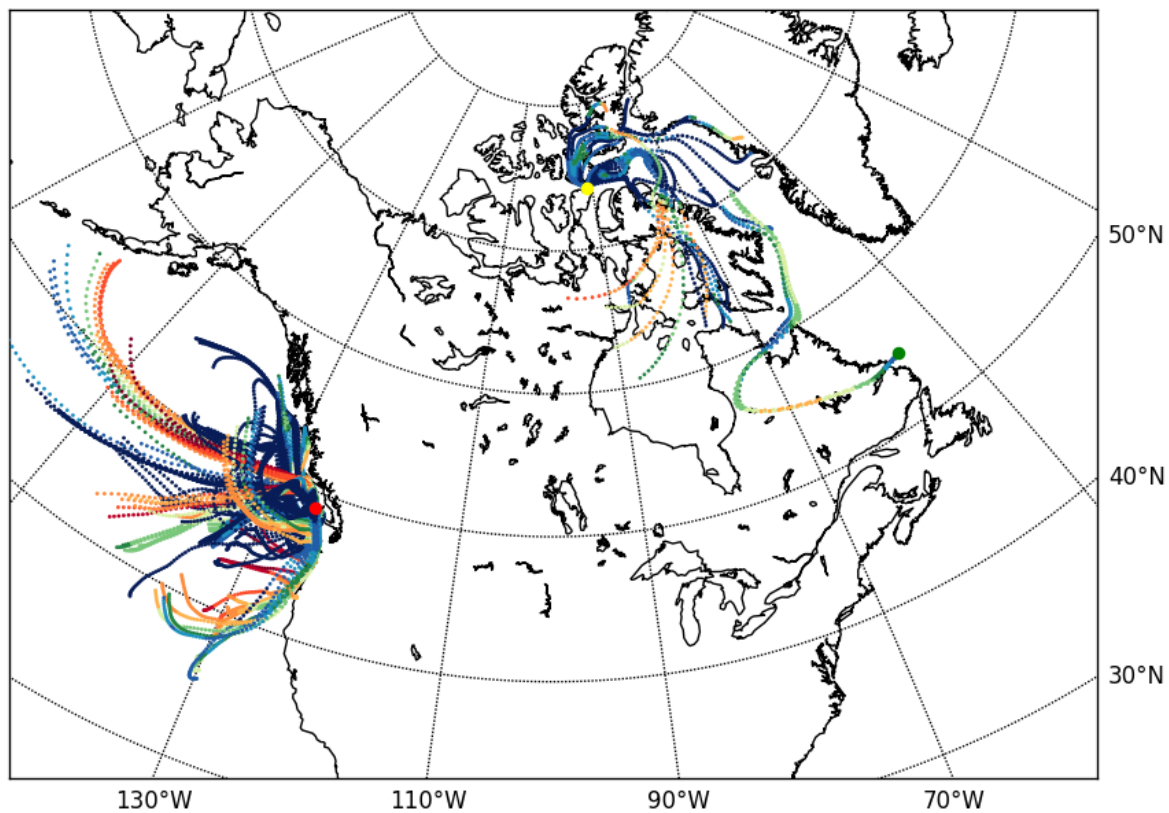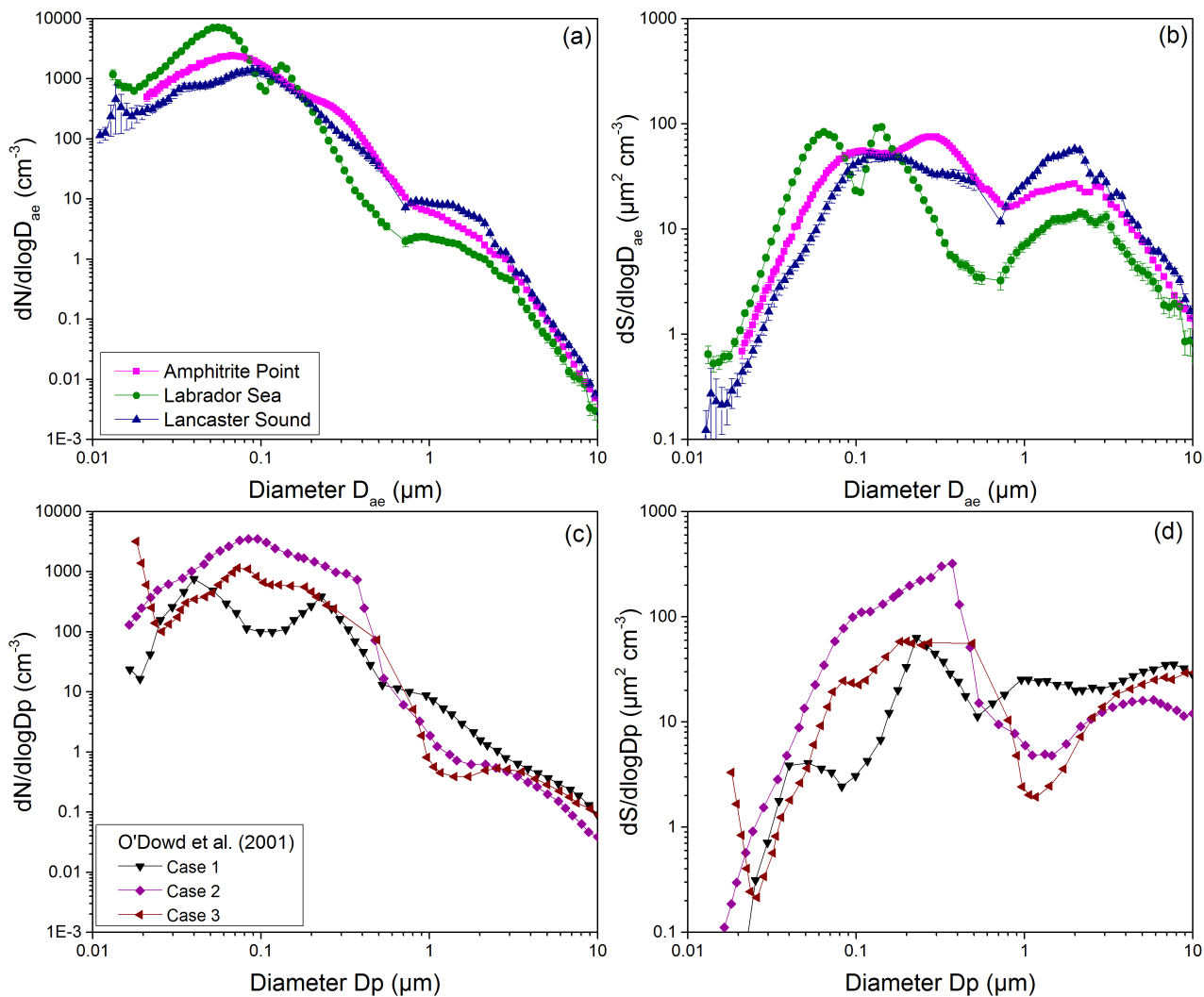
6

Figure S2. The 3-day HYSPLIT back trajectories initiating at 150 m above ground level for Amphitrite Point (red dot), Labrador Sea (green dot) and Lancaster Sound (yellow dot). The back trajectories were calculated for every hour during the MOUDI sampling period. The starting points are labeled as coloured dots, and the altitude is shown using a colour scale.

Figure S3. Comparison of the average aerosol particle number and surface area size distributions measured during MOUDI sampling periods in this study (a, b) with the average aerosol particle number and surface area size distributions measured at a mid-latitude North-Atlantic marine boundary layer site (c, d) (O'Dowd et al., 2001)**. Case 1 from** O'Dowd et al. (2001) **corresponds to clean marine air measured under moderate humidity (80 %) and wind speeds (6 m s^{-1}) conditions, Case 2 corresponds to anthropogenically influenced maritime air measured at wind speeds in the order of 2-4 m s^{-1}, and Case 3 corresponds to anthropogenically influenced maritime air during a nucleation burst measured at wind speeds of 4 m s^{-1}.**
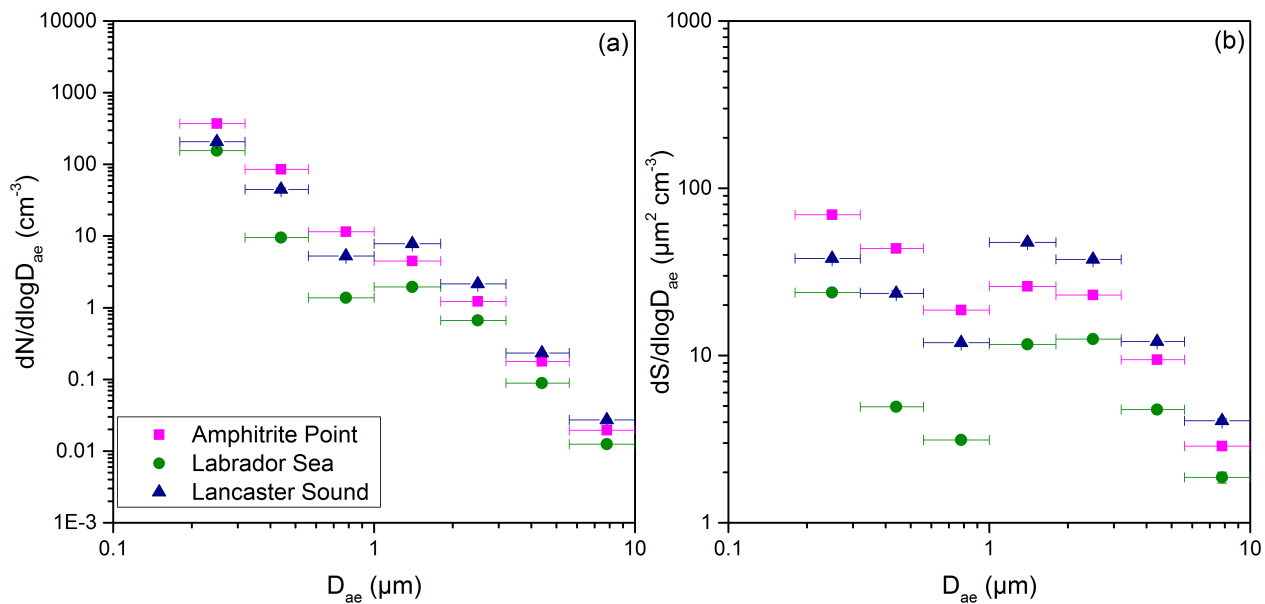
Figure S4. Concentrations of (a) aerosol number, *N*, and (b) surface area, *S*, as a function of aerodynamic diameter, D_{ae}, using the same bin widths as the MOUDI. Each data point was calculated by averaging the numbers from Fig. 4 that were within the corresponding size bin. The plotted x-values represent the midpoints of the size bins from the MOUDI. The x-error bars represent the widths of the size bins, and the y-error bars are propagated uncertainties from the error bars in Fig. 4. In most cases, the y-error bars are smaller than the size of the symbols.
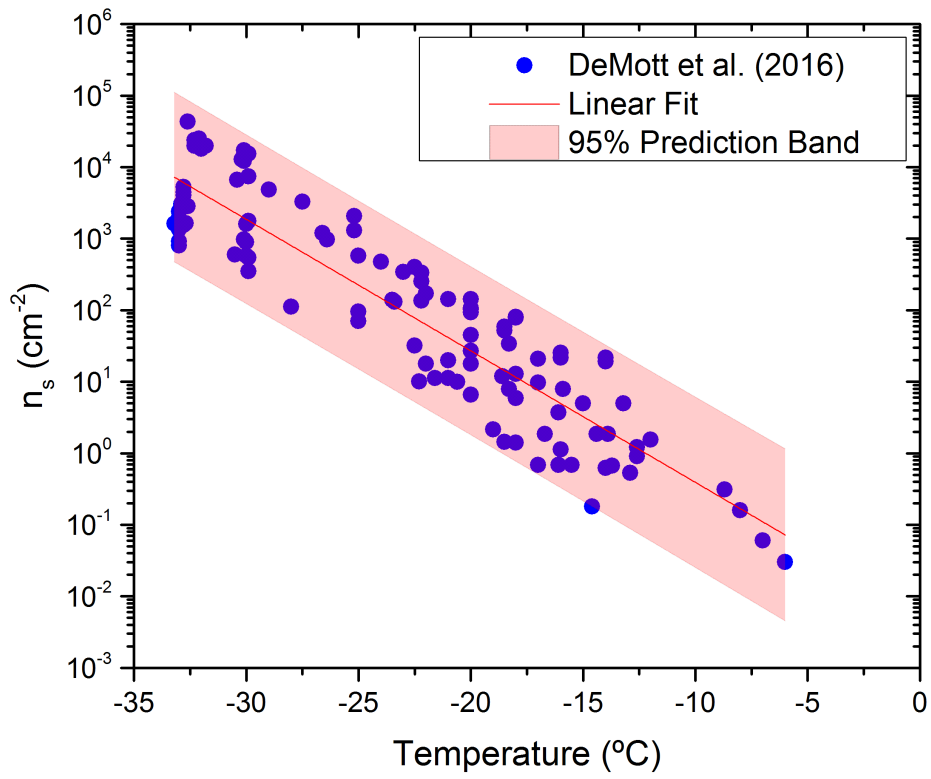
Figure S5. n_s values of sea spray aerosol as a function of temperature taken from DeMott et al. (2016). Shown is a linear fit to the data and 95% prediction bands.
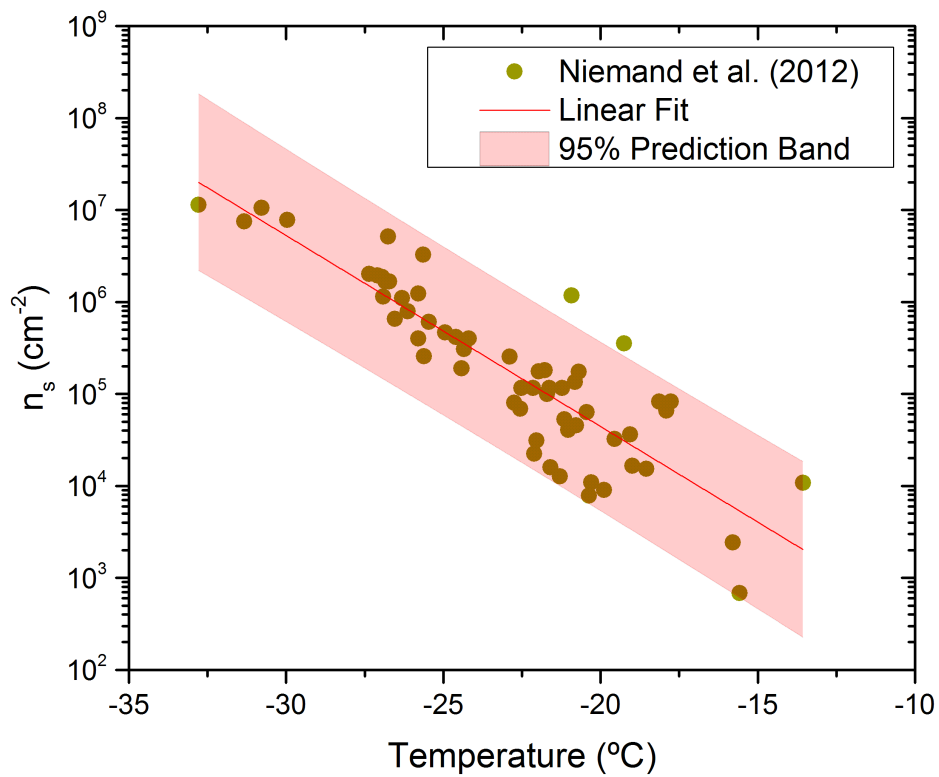
Figure S6. n_s values of mineral dust as a function of temperature taken from Niemand et al. (2012). Shown is a linear fit to the data and 95% prediction bands.
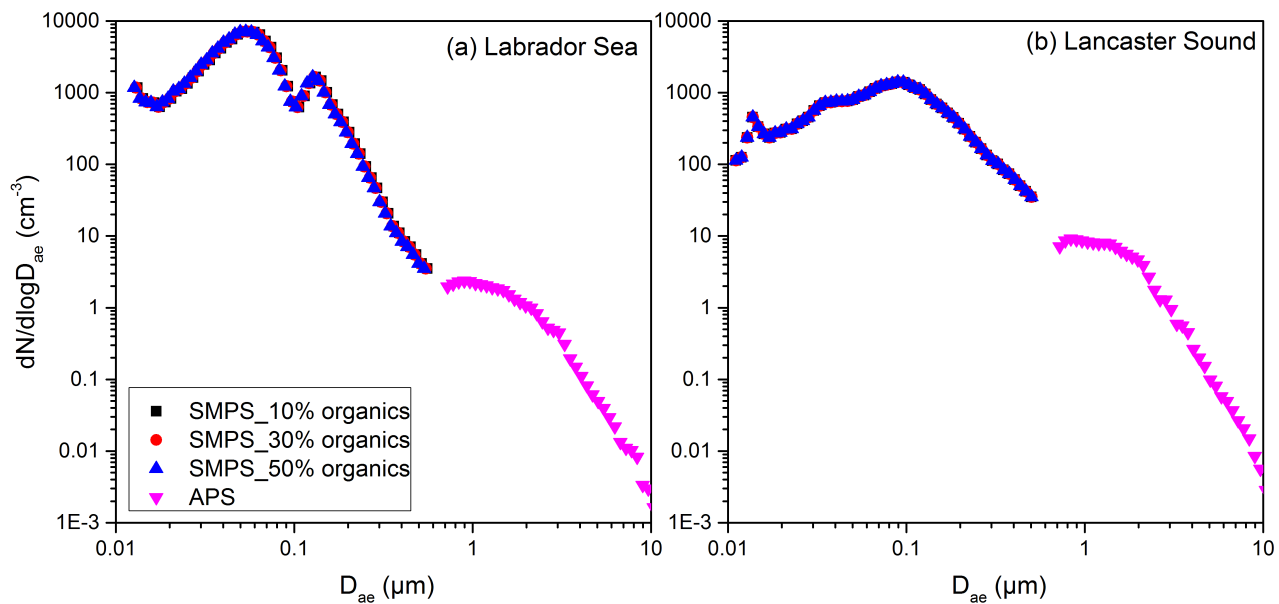
Figure S7. The average number size distribution measured at Labrador Sea (a) and Lancaster Sound (b) with the mobility diameter measured by the SMPS converted to aerodynamic diameter assuming a sea spray aerosol with 10 %, 30 %, and 50 % organic mass content.